Journal of Materials Chemistry A

PAPER

View Article Online
View Journal | View Issue

Cite this: J. Mater. Chem. A, 2015, 3, 21337

Ultrathin MnO_2 nanoflakes grown on N-doped carbon nanoboxes for high-energy asymmetric supercapacitors†

Yihui Dai,[a] Ling Chen,[a] Vladimir Babayan,[b] Qilin Cheng,[a] Petr Saha,[b] Hao Jiang*[a] and Chunzhong Li*[a]

Received 2nd September 2015
Accepted 14th September 2015

DOI: 10.1039/c5ta06958k

www.rsc.org/MaterialsA

We demonstrate the synthesis of ultrathin MnO_2 nanoflakes grown on N-doped carbon nanoboxes, forming an impressive hierarchical MnO_2/C nanobox hybrid with an average size of 500 nm, which exhibits an excellent electrochemical performance due to the unique structure, N-doping and strong synergistic effects between them. In addition, we also assembled a green asymmetric supercapacitor (ASC) using the as-synthesized MnO_2/C nanoboxes as a positive electrode and the corresponding N-doped carbon nanoboxes as a negative electrode in a neutral aqueous electrolyte, aiming to further enhance its energy density by extending the operating potential. More significantly, our ASC device is able to reversibly cycle within a wide operating voltage of 2.0 V and delivers a maximum energy density of 39.5 W h kg^{-1} with superior cycling stability (~90.2% capacitance retention after 5000 cycles). These intriguing results show that hollow nanostructures will be promising electrode materials for advanced supercapacitors.

Introduction

In recent years, considerable attention has been paid to hollow nanostructures owing to their attractive properties such as high surface area, low effective density, low coefficients of thermal expansion and good permeation, which render them promising candidates for applications in energy storage, catalysis, adsorption materials, drug delivery, and some others.[1–4] As for supercapacitors, a promising power source for portable electronic devices and electric vehicles (EVs) owing to their intriguing merits of high power density, long lifespan and environmental friendliness, many hollow structured electrode materials have been widely exploited, achieving a higher energy/power density indeed.[5–7] However, their electrochemical performances, especially energy densities, are still unsatisfactory to meet the requirement of practical applications.[8–10] Therefore, to further improve the energy density of supercapacitors, we need to design and synthesize novel hollow nanostructured electrode materials. On the other hand, according to equation $E = C(\Delta V)^2/2$, another effective strategy is to maximize the operating voltage (ΔV).[11,12] In this regard, organic electrolytes or ionic liquids are developed to provide a wider potential window, but these nonaqueous media usually suffer from poor conductivity, high cost and safety concerns.[13] Thankfully, asymmetric supercapacitors (ASCs) are a rather wise choice, particularly in neutral aqueous electrolytes, which will remarkably improve the energy density in virtue of the extended operating potential, but also meet the demand of green electrolytes.[14–16] It is noted that high energy/power densities will be achieved if we can develop high performance positive and negative electrode materials and meanwhile assemble them into ASC devices accordingly.[17]

Thus far, manganese oxide (MnO_2) has been extensively studied as an electrode material for supercapacitors owing to its high theoretical specific capacitance, environmental benignity and low cost.[18–21] More impressively, MnO_2 has a wide potential window in neutral aqueous electrolytes, making it more appealing than other metal oxides (*e.g.* NiO and Co_3O_4) usually used in strong acidic or alkaline electrolytes. However, pure MnO_2 typically suffers from poor conductivity (10^{-5} to 10^{-6} S cm^{-1}), which crucially depresses its practical capacity delivery.[22] To address this issue, a general strategy is to prepare nanostructured MnO_2 supported on conductive carbon substrates.[23–25] For example, Chen *et al.*[26] reported the synthesis of a bacterial-cellulose-derived carbon nanofiber@MnO_2 (p-BC@MnO_2) composite, which was then assembled into an ASC device in 1 M Na_2SO_4 aqueous solution using the corresponding p-BC as the negative electrode, showing an enhanced energy density of 32.9 W h kg^{-1}. In addition, hetero-atom doping can introduce extra reversible pseudo-capacitance and enhance the electrical conductivity of carbon materials.[27,28]

[a]Key Laboratory for Ultrafine Materials of Ministry of Education, School of Materials Science and Engineering, East China University of Science and Technology, Shanghai 200237, China. E-mail: jianghao@ecust.edu.cn; czli@ecust.edu.cn; Fax: +86-21-64250624; Tel: +86-21-64250949

[b]Centre of Polymer Systems, University Institute, Tomas Bata University in Zlin, Trida T. Bati 5678, 760 01 Zlin, Czech Republic

† Electronic supplementary information (ESI) available. See DOI: 10.1039/c5ta06958k

Herein, we demonstrate the synthesis of novel hierarchical MnO_2/C hollow nanostructures comprised of ultrathin MnO_2 nanoflakes on N-doped carbon nanoboxes by using Fe_2O_3 nanocubes as a template and dopamine as a carbon source. An ASC device has been assembled in 1 M Na_2SO_4 aqueous solution based on the as-obtained MnO_2/C nanoboxes as a positive electrode and the corresponding N-doped carbon nanoboxes as a negative electrode. As expected, the as-fabricated ASC device has a wide and stable operating voltage of 2.0 V, and an energy density as high as 39.5 W h kg^{-1} can be achieved with superior cycling stability (90.2% capacitance retention after 5000 cycles). Therefore, the design and synthesis of hollow nanostructures will promote the rapid development of advanced supercapacitors.

Experimental

Material synthesis

Synthesis of N-doped carbon nanoboxes. Fe_2O_3 nanocubes, as a template, were firstly synthesized according to Lou's work.[29] And then, 80 mg of the as-obtained Fe_2O_3 nanocubes was dispersed in 100 mL of 10 mM 2-amino-2-hydroxymethyl-propane-1,3-diol (Tris) solution. After that, 40 mg of dopamine was added into the mixture with magnetic stirring for 5 h. The products, *i.e.* Fe_2O_3@PDA, were collected and washed several times with deionized water and ethanol before drying at 70 °C. Finally, the N-doped carbon nanoboxes were obtained by annealing the Fe_2O_3@PDA nanocubes under Ar and subsequent acid etching of the core templates.

Synthesis of MnO_2/C nanoboxes. In a typical synthesis, 0.1 g of the above obtained N-doped carbon nanoboxes was dispersed into 50 mL of 0.1 M $KMnO_4$ solution under stirring at 40 °C for 2 h. Subsequently, 10 mL of 0.2 M $Mn(NO_3)_2$ solution was added dropwise into the as-mentioned mixture with vigorous stirring for another 21 h. Then, the MnO_2/C nanoboxes were collected, by filtration, washed several times with deionized water and alcohol, and dried at 70 °C overnight.

Material characterization

The structure and morphology of the as-prepared products were characterized with an X-ray powder diffractometer (XRD, Rigaku D/Max2550, Cu Kα radiation) at a scan rate of 1° min^{-1}, a scanning electron microscope (FESEM, Hitachi S-4800), and a transmission electron microscope (TEM, JEOL-2100F) operating at 200 kV. X-ray photoelectron spectroscopy (XPS) spectra and the Raman spectrum were recorded with an AXIS Ultra DLD spectrometer (Al Kα X-ray source) and a NEXUS 670 FT-IR Raman spectrometer, respectively. N_2 adsorption/desorption was carried out by Brunauer–Emmett–Teller (BET) measurements using a Micromeritics ASAP 2010 analyzer.

Electrochemical measurements

Electrochemical evaluation was carried out in 1 M Na_2SO_4 aqueous solution on an Autolab PGSTAT302N potentiostat electrochemical workstation. The electrode was prepared by mixing the active material, acetylene black and polyvinylidene fluoride (PVDF) at a ratio of 8 : 1 : 1 in NMP solvent. Then the as-formed slurry was coated onto graphite paper (1 cm^2) using a doctor blade method and dried at 120 °C for 2 h. The ASC device was built based on MnO_2/C nanoboxes as a positive electrode and N-doped carbon nanoboxes as a negative electrode with a glassy fibrous separator, which was then investigated using a two-electrode configuration in 1 M Na_2SO_4 aqueous electrolyte. Prior to constructing the ASC device, the mass ratio of positive and negative electrode materials was determined to be about $m_+/m_- = 0.78$ based on the specific capacitance values calculated from their CV results in a three-electrode system. The weights were 0.77 mg and 0.98 mg, respectively, for positive and negative electrodes. The specific capacitance of the ASC was calculated based on the total mass of both electrodes.

Results and discussion

The synthesis process of hierarchical MnO_2/C nanoboxes is illustrated in Scheme 1. The carbon nanoboxes were first synthesized according to Lou's work[29] with a minor revision. Speaking in detail, uniform Fe_2O_3 nanocubes with an average size of 500 nm as templates were first synthesized for the coating of carbon source polydopamine (PDA); the corresponding SEM images are shown in Fig. S1.† After carbonization and acid etching of the Fe_2O_3 core, the N-doped carbon nanoboxes were obtained, as shown in Fig. 1a, which are intact and uniform with a mean size of about 500 nm. The corresponding TEM image (Fig. 1b) demonstrates that these carbon nanoboxes possess a hollow nanostructure with a uniform shell thickness of about 20 nm. Notably, the hollow inner space of N-doped carbon nanoboxes can serve as the "buffering reservoir" for fast ion transport during the rapid charge/discharge process. Meanwhile, we also realize the ultrathin MnO_2 nanoflakes grown on N-doped carbon nanoboxes by a simple strategy, forming the hierarchical MnO_2/C nanoboxes. Fig. 1c shows the corresponding SEM image of the as-prepared MnO_2/C nanoboxes. It can be seen that a layer of MnO_2 has been entirely and uniformly grown on the surface of N-doped carbon nanoboxes. The high-magnification SEM image of a representative MnO_2/C nanobox (Fig. S2†) reveals that the MnO_2 layer is randomly assembled by numerous ultrathin MnO_2 nanoflakes. The detailed microstructure of the MnO_2/C nanoboxes was further characterized by TEM, as shown in Fig. 1d–f. Fig. 1d confirms the homogeneous coverage of MnO_2 on N-doped carbon nanoboxes, which agrees well with SEM observation. The high-magnification TEM image (Fig. 1e) clearly shows that ultrathin MnO_2 nanoflakes are directly grown on the surface of carbon substrates with lengths of about 20 nm. Such ultrathin MnO_2

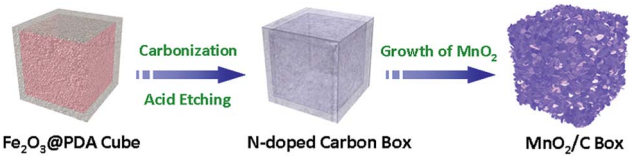

Scheme 1 Schematic illustration of the synthesis process of the as-obtained MnO_2/C nanoboxes.

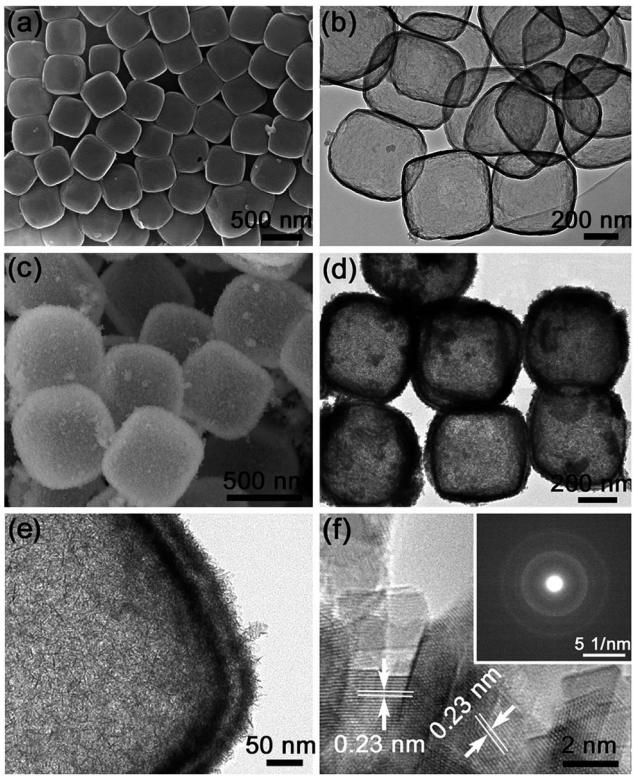

Fig. 1 (a) SEM and (b) TEM images of the N-doped carbon nanoboxes. (c) SEM, (d and e) TEM and (f) HRTEM images of the MnO_2/C nanoboxes. The inset of (f) shows the SAED pattern of the ultrathin MnO_2 nanoflakes.

nanostructures possess enhanced accessibility to the electrolyte, ensuring high electrochemical utilization of active materials. From the high-resolution TEM (HRTEM) image (Fig. 1f), we can see the clear lattice fringes of MnO_2 nanoflakes which are calculated to be about 0.23 nm. The selected area electronic diffraction (SAED) pattern (inset of Fig. 1f), taken from a random MnO_2 nanoflake, shows a polycrystalline nature.

To analyze the chemical composition and oxidation state of Mn in the as-prepared MnO_2/C composite, X-ray photoelectron spectroscopy (XPS) was conducted. The spectrum (Fig. 2a) shows the signals of Mn, O, C and N elements, implying the presence of MnO_2 and successful doping of nitrogen which comes from the carbon precursor dopamine. The high-resolution Mn 2p spectrum (left inset of Fig. 2a) shows a Mn $2p^{3/2}$ peak at 642.0 eV and a Mn $2p^{1/2}$ peak at 653.7 eV with a spin-energy separation of 11.7 eV, being in good agreement with those reported for MnO_2.[22,30] The N 1s peak (right inset of Fig. 2a) can be resolved into three components centered at 398.4, 400.7, and 403.5 eV, corresponding to pyridinic (*N*-6), quaternary (*N*-Q), and graphitic types of nitrogen, respectively.[31,32] It is reported that the nitrogen atoms can improve the wettability of active materials in the electrolyte and thus favor the ion transport.[32,33] Moreover, the presence of *N*-Q and *N*-6 is beneficial to the conductivity and extra pseudocapacitance of carbon materials.[34] To further confirm the crystalline phase of the ultrathin MnO_2 nanoflakes, X-ray diffraction (XRD) analysis was carried out. Fig. 2b shows the XRD patterns of MnO_2/C nanoboxes together with the corresponding N-doped carbon nanoboxes, in which the broad peak at about 26° for both samples is a typical characteristic of high graphitization carbon, while the diffraction peaks at 28.7°, 37.6°, 42.0°, 47.2°, 56.2°, 59.5° and 65.5° can be well assigned to the (310), (121), (301), (510), (600), (260) and (002) planes of the tetragonal α-MnO_2 phase (JCPDS no. 72-1982).[35] The Raman spectrum was also measured to analyze the carbon quality in MnO_2/C nanoboxes. As shown in Fig. 2c, two strong peaks can be found at 1358 and 1597 cm^{-1}, corresponding to the disordered D band and graphitic G band of carbon, respectively.[36] The intensity ratio I_D/I_G is calculated to be 0.88, indicating a high graphitization degree. In addition, our MnO_2/C nanoboxes also possess a high BET surface area of 130 $m^2\ g^{-1}$ (Fig. S3†). Such intriguing features are beneficial for the rapid transportation of ions/electrons, leading to high energy/power densities.

To evaluate the electrochemical potential windows and quantify the specific capacitance values of N-doped carbon nanoboxes and MnO_2/C nanoboxes, cyclic voltammogram (CV) measurements were first carried out using a three-electrode configuration in 1 M Na_2SO_4 electrolyte. The N-doped carbon and MnO_2/C electrodes were tested within the potential window of −1.0 to 0.2 V and 0–1.0 V, respectively, at a scan rate of 20 mV s^{-1}. As shown in Fig. 3a, the relatively rectangular shapes of the CV curves without noticeable redox peaks indicate the good capacitive behavior for both electrodes. A series of galvanostatic charge/discharge tests were also conducted for both electrodes within the above potential windows at different current densities, as shown in Fig. S4.† The almost linear and triangular shapes further demonstrate the rapid current response and excellent electrochemical reversibility. The electrochemical performances are also better, at least comparable to the related studies in the literature.[37–40] Thus, the stable operating potential window can be defined for the N-doped carbon electrode (−1.0 to 0.2 V) and MnO_2/C electrode (0–1.0 V) with capacitive

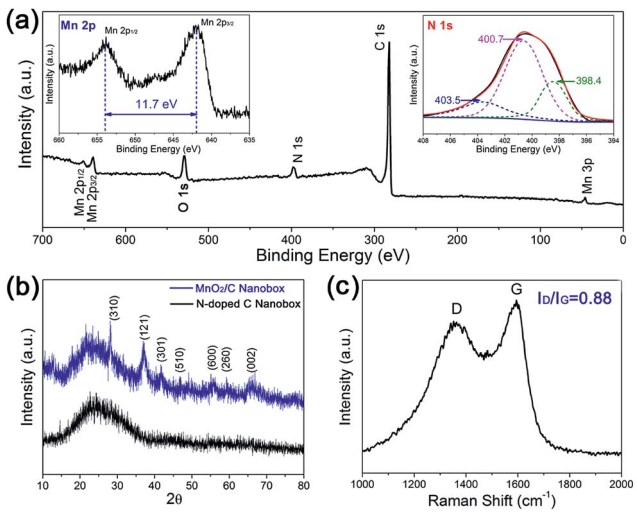

Fig. 2 (a) XPS spectrum, (b) XRD patterns and (c) Raman spectrum of MnO_2/C nanoboxes. The insets of (a) show the high-resolution spectra of Mn 2p and N 1s, respectively.

behavior. In this context, an extended operating voltage of 2.0 V is expected to be achieved when assembling an ASC device using the lower cutoff voltage of N-doped carbon (−1.0 V, negative electrode) and the higher cutoff voltage of MnO_2/C (1.0 V, positive electrode), as shown in Fig. S5.†

Prior to constructing the ASC device, the mass ratio of positive and negative electrodes (m_+/m_-) should be optimized based on the charge balance theory: $q_+ = q_-$ ($q = C \times \Delta E \times m$), where C, m, and ΔE represent the specific capacitance, loading mass, and potential range of each electrode.[41] Based on the specific capacitance values calculated from the corresponding CV curves (Fig. 3a), which are 187 and 288 F g^{-1} for N-doped carbon and MnO_2/C, respectively, the optimal mass ratio of m_+/m_- will be 0.78 in the present ASC device.

Fig. 3b shows the CV curves of the as-fabricated ASC device within different potential windows ranging from 1.0 to 2.0 V in 1 M Na_2SO_4 electrolyte at a scan rate of 20 mV s^{-1}. As expected, CV curves at all potential windows showed quasi-rectangular and symmetric shapes, implying that the present ASC device possesses ideal capacitive behavior within a wide and stable operating voltage up to 2.0 V in neutral aqueous medium. It is known that the energy density is proportional to the square of voltage, so the enlarged operating voltage will lead to a remarkably enhanced energy density of supercapacitors.

Fig. 4a provides the galvanostatic charge/discharge curves recorded at various current densities of 0.2–2 A g^{-1} from which the rate performance of the as-fabricated ASC device can be evaluated. The typical triangular shapes of the charge/discharge curves exhibit considerable linear slopes with good symmetry at all current densities, indicating the good capacitive characteristics and fast charging/discharging profile of the ASC cell. A high specific capacitance of 71 F g^{-1} is achieved at 0.2 A g^{-1} for the ASC device calculated from the discharge curve, which still retains 42.4 F g^{-1} at 2 A g^{-1} with a capacitance retention of 60%, as shown in Fig. 4b, indicating a good rate performance. Moreover, the present ASC also possesses excellent cycling stability. As shown in Fig. 4c, a high capacitance retention of 90.2% is achieved after 5000 cycles performed at a current density of 2 A g^{-1}. A Ragone plot derived from various discharge curves is provided to highlight the energy density *vs.* power density of the present ASC device, as shown in Fig. 4d. The as-prepared ASC cell shows a high energy density of 39.5 W h kg^{-1} at a power density of 200 W kg^{-1}, which still retains 23.1 W h kg^{-1} at a high power density of 2000 W kg^{-1}. This value also exceeds those of MnO_2-based ASC devices with the aqueous electrolyte reported previously, such as MnO_2/graphene//graphene (30.4 W h kg^{-1} at 100 W kg^{-1}),[19] MnO_2/GO//hierarchical porous carbon (34.4 W h kg^{-1} at 200 W kg^{-1}),[42] MnO_2/carbon nanofiber//activated carbon nanofiber (30.6 W h kg^{-1} at 200 W kg^{-1})[43] and MnO_2/graphitic hollow carbon spheres (GHCS-MnO_2)//GHCS (22 W h kg^{-1} at 100 W kg^{-1}).[44] In a previous study, an ASC device based on petal-shaped MnO_2 nanosheets as the positive electrode and a network of CNT–carbon nanofibers as the negative electrode was assembled by Wang *et al.*, which delivered a very high energy density of 52.22 W h kg^{-1} at 100 W kg^{-1} in 0.5 M Na_2SO_4 electrolyte, but only 2000 cycles were accomplished in the cycling test with apparent capacity fading in the last several hundred cycles.[45] These intriguing results demonstrate that the green ASC in our work can simultaneously achieve high energy density and excellent cycling stability.

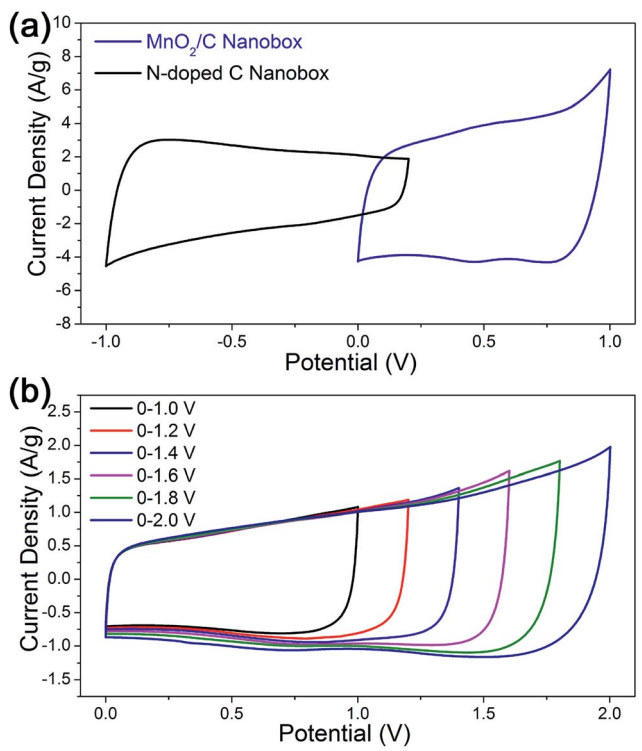

Fig. 3 (a) CV curves of the N-doped carbon and the MnO_2/C electrodes performed in a three-electrode configuration in 1 M Na_2SO_4 electrolyte at a scan rate of 20 mV s^{-1}. (b) CV curves of the as-fabricated ASC device measured at different potential windows in 1 M Na_2SO_4 electrolyte at a scan rate of 20 mV s^{-1}.

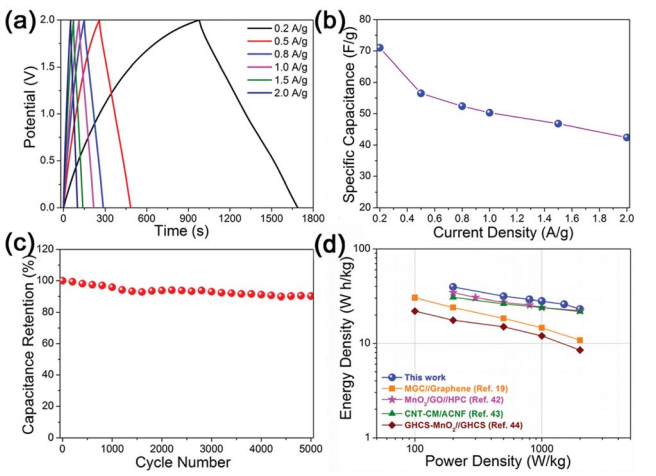

Fig. 4 (a) Charge/discharge curves of the as-fabricated ASC device at different current densities. (b) The specific capacitance as a function of the current densities. (c) The capacitance retention as a function of cycle number at a current density of 2 A g^{-1}. (d) Ragone plots of the present ASC device and other reported MnO_2-based ASC devices.

The outstanding performance of the present ASC device could be attributed to the unique hollow nanostructures and the appropriate combination of each electrode component: (i) the N-doped carbon nanobox substrate is highly conductive to enhance the electron transport to the outer MnO_2 layer, (ii) the ultrathin MnO_2 nanoflakes possess abundant electroactive sites for the migration of electrolyte ions, leading to the effective utilization of active materials. Furthermore, the hydrophilic effect of N-doping also allows better access to the electrolyte, (iii) the hollow interiors can act as the ion reservoir to ensure the consecutive supply of the electrolyte even at high rates, further shortening the ion diffusion paths, and (iv) the directly grown MnO_2 nanoflakes have close adhesion to the carbon substrate, ensuring the strong integrity of hierarchical MnO_2/C nanoboxes and cycling stability. The above attractive findings demonstrate that the present ASC device based on hollow nanostructures would hold great potential as a green candidate for high-energy supercapacitors.

Conclusions

In conclusion, we have demonstrated the synthesis of a novel hierarchical MnO_2/C hollow nanostructure by the growth of ultrathin MnO_2 nanoflakes on N-doped carbon nanoboxes using Fe_2O_3 nanocubes as a template and dopamine as a carbon source, which exhibits excellent electrochemical performance due to the unique structure, N-doping and strong synergistic effects between them. To further enhance the energy density, a green ASC device has been assembled with a neutral aqueous electrolyte based on the as-prepared MnO_2/C nanoboxes as a positive electrode and the corresponding N-doped carbon nanoboxes as a negative electrode. As expected, the as-fabricated ASC device can be operated reversibly in a wide potential range between 0 and 2.0 V in 1 M Na_2SO_4 aqueous electrolyte and deliver a maximum energy density as high as 39.5 W h kg^{-1} at a power density of 200 W kg^{-1}. Furthermore, the present ASC device also exhibits superior cycling stability with 90.2% capacitance retention after 5000 cycles. These results will provide more insight into the development of hollow nanostructures for advanced supercapacitors.

Acknowledgements

This work was supported by the National Natural Science Foundation of China (21206043, 21236003, 21371057), the Basic Research Program of Shanghai (13NM1400801), the International Science and Technology Cooperation Program of China (2015DFA51220), the 111 Project (B14018), and the Fundamental Research Funds for the Central Universities. Authors V. B. and P. S. appreciate the financial support of the Ministry of Education, Youth and Sports of the Czech Republic – Program NPU I (LO1504).

Notes and references

1 S. H. Im, U. Y. Jeong and Y. N. Xia, *Nat. Mater.*, 2005, **4**, 671–675.
2 X. Y. Lai, J. E. Halpert and D. Wang, *Energy Environ. Sci.*, 2012, **5**, 5604–5618.
3 H. Jiang, J. Ma and C. Z. Li, *Adv. Mater.*, 2012, **24**, 4197–4202.
4 J. Liu, S. Z. Qiao, S. B. Hartono and G. Q. Lu, *Angew. Chem., Int. Ed.*, 2010, **122**, 5101–5105.
5 Y. Munaiah, B. G. S. Raj, T. P. Kumar and P. Ragupathy, *J. Mater. Chem. A*, 2013, **1**, 4300–4306.
6 T. Zhu, Z. Y. Wang, S. J. Ding, J. S. Chen and X. W. Lou, *RSC Adv.*, 2011, **1**, 397–400.
7 W. Du, R. M. Liu, Y. W. Jiang, Q. Y. Lu, Y. Z. Fan and F. Gao, *J. Power Sources*, 2013, **227**, 101–105.
8 H. Jiang, D. Y. Ren, H. F. Wang, Y. J. Hu, S. J. Guo, H. Y. Yuan, P. J. Hu, L. Zhang and C. Z. Li, *Adv. Mater.*, 2015, **27**, 3687–3695.
9 Y. Hou, Y. W. Cheng, T. Hobson and J. Liu, *Nano Lett.*, 2010, **10**, 2727–2733.
10 H. Jiang, P. S. Lee and C. Z. Li, *Energy Environ. Sci.*, 2013, **6**, 41–53.
11 E. R. Pinero, F. Leroux and F. Beguin, *Adv. Mater.*, 2006, **18**, 1877–1882.
12 L. L. Zhang and X. S. Zhao, *Chem. Soc. Rev.*, 2009, **38**, 2520–2531.
13 H. C. Gao, F. Xiao, C. B. Ching and H. W. Duan, *ACS Appl. Mater. Interfaces*, 2012, **4**, 2801–2810.
14 Z. Fan, J. Yan, T. Wei, L. Zhi, G. Ning, T. Li and F. Wei, *Adv. Funct. Mater.*, 2011, **21**, 2366–2375.
15 B. G. Choi, M. Yang, W. H. Hong, J. W. Choi and Y. S. Huh, *ACS Nano*, 2012, **6**, 4020–4028.
16 H. Jiang, C. Z. Li, T. Sun and J. Ma, *Nanoscale*, 2012, **4**, 807–812.
17 X. Zhao, L. L. Zhang, S. Murali, M. D. Stoller, Q. H. Zhang, Y. W. Zhu and R. S. Ruoff, *ACS Nano*, 2012, **6**, 5404–5412.
18 M. J. Zhi, C. C. Xiang, J. T. Li, M. Li and N. Q. Wu, *Nanoscale*, 2013, **5**, 72–88.
19 Z. S. Wu, W. C. Ren, D. W. Wang, F. Li, B. L. Liu and H. M. Cheng, *ACS Nano*, 2010, **4**, 5835–5842.
20 Y. Hou, Y. W. Cheng, T. Hobson and J. Liu, *Nano Lett.*, 2010, **10**, 2727–2733.
21 W. F. Wei, X. W. Cui, W. X. Chen and D. G. Ivey, *Chem. Soc. Rev.*, 2011, **40**, 1697–1721.
22 S. W. Lee, J. Kim, S. Chen, P. T. Hammond and Y. Shao-Horn, *ACS Nano*, 2010, **4**, 3889–3896.
23 S. Chen, J. W. Zhu, X. D. Wu, Q. F. Han and X. Wang, *ACS Nano*, 2010, **4**, 2822–2830.
24 H. Zhang, G. P. Cao, Z. Y. Wang, Y. S. Yang, Z. J. Shi and Z. N. Gu, *Nano Lett.*, 2008, **8**, 2664–2668.
25 J. Ge, H. B. Yao, W. Hu, X. F. Yu, Y. X. Yan, L. B. Mao, H. H. Li, S. S. Li and S. H. Yu, *Nano Energy*, 2013, **2**, 505–513.
26 L. F. Chen, Z. H. Huang, H. W. Liang, Q. F. Guan and S. H. Yu, *Adv. Mater.*, 2013, **25**, 4746–4752.
27 P. J. Hall, M. Mirzaeian, S. Isobel Fletcher, F. B. Sillars, A. J. R. Rennie, G. O. Shitta-Bey, G. Wilson, A. Cruden and R. Carter, *Energy Environ. Sci.*, 2010, **3**, 1238–1251.
28 S. H. Yang, X. F. Song, P. Zhang and L. Gao, *ACS Appl. Mater. Interfaces*, 2013, **5**, 3317–3322.
29 X. Y. Yu, H. Hu, Y. W. Wang, H. Y. Chen and X. W. Lou, *Angew. Chem., Int. Ed.*, 2015, **54**, 7395–7398.

30 A. L. M. Reddy, M. M. Shaijumon, S. R. Gowda and P. M. Ajayan, *Nano Lett.*, 2009, **9**, 1002–1006.
31 Y. M. Tan, C. F. Xu, G. X. Chen, Z. H. Liu, M. Ma, Q. J. Xie, N. F. Zheng and S. Z. Yao, *ACS Appl. Mater. Interfaces*, 2013, **5**, 2241–2248.
32 F. Su, C. K. Poh, J. S. Chen, G. Xu, D. Wang, Q. Li, J. Lin and X. W. Lou, *Energy Environ. Sci.*, 2011, **4**, 717–724.
33 H. Guo and Q. Gao, *J. Power Sources*, 2009, **186**, 551–556.
34 W. R. Li, D. H. Chen, Z. Li, Y. F. Shi, Y. Wan, J. J. Huang, J. J. Yang, D. Y. Zhao and Z. Y. Jiang, *Electrochem. Commun.*, 2007, **9**, 569–573.
35 Y. Liu, M. Zhang, J. H. Zhang and Y. T. Qian, *J. Solid State Chem.*, 2006, **179**, 1757–1761.
36 H. Jiang, Y. J. Hu, S. J. Guo, C. Y. Yan, P. S. Lee and C. Z. Li, *ACS Nano*, 2014, **8**, 6038–6046.
37 P. C. Chen, G. Z. Shen, Y. Shi, H. T. Chen and C. W. Zhou, *ACS Nano*, 2010, **4**, 4403–4411.
38 M. Yang, Y. Zhong, X. Zhou and Z. Zhou, *J. Mater. Chem. A*, 2014, **2**, 12519–12525.
39 L. Li, R. M. Li, S. L. Gai, S. J. Ding, F. He, M. L. Zhang and P. P. Yang, *Chem.–Eur. J.*, 2015, **21**, 7119–7126.
40 M. Yang, Y. R. Zong, J. Bao, X. L. Zhou and Z. Zhou, *J. Mater. Chem. A*, 2015, **3**, 11387–11394.
41 M. Yang, Y. R. Zong, L. W. Su, J. P. Wei and Z. Zhou, *Chem.–Eur.J.*, 2014, **20**, 5046–5053.
42 Y. F. Zhao, W. Ran, J. He, Y. Z. Huang, Z. F. Liu, W. Liu, Y. F. Tang, L. Zhang, D. W. Gao and F. M. Gao, *Small*, 2015, **11**, 1310–1319.
43 J. G. Wang, Y. Yang, Z. H. Huang and F. Y. Kang, *Carbon*, 2013, **61**, 190–199.
44 Z. B. Lei, J. T. Zhang and X. S. Zhao, *J. Mater. Chem.*, 2012, **22**, 153–160.
45 C. H. Wang, H. C. Hsu and J. H. Hu, *J. Power Sources*, 2014, **249**, 1–8.